BRAIN
ORIGINAL ARTICLE

Intravenous delivery of adeno-associated viral gene therapy in feline GM1 gangliosidosis

Amanda L. Gross,[1,2] Heather L. Gray-Edwards,[1,†] Cassie N. Bebout,[1] Nathan L. Ta,[3] Kayly Nielsen,[1] Brandon L. Brunson,[2] Kalajan R. Lopez Mercado,[1] Devin E. Osterhoudt,[1] Ana Rita Batista,[4,5] Stacy Maitland,[4,5] Thomas N. Seyfried,[3] Miguel Sena-Esteves[4,5] and Douglas R. Martin[1,2]

GM1 gangliosidosis is a fatal neurodegenerative disease caused by a deficiency of lysosomal β-galactosidase. In its most severe form, GM1 gangliosidosis causes death by 4 years of age, and no effective treatments exist. Previous work has shown that injection of the brain parenchyma with an adeno-associated viral (AAV) vector provides pronounced therapeutic benefit in a feline GM1 model. To develop a less invasive treatment for the brain and increase systemic biodistribution, intravenous injection of AAV9 was evaluated.

AAV9 expressing feline β-galactosidase was intravenously administered at 1.5×10^{13} vector genomes/kg body weight to six GM1 cats at ~1 month of age. The animals were divided into two cohorts: (i) a long-term group, which was followed to humane end point; and (ii) a short-term group, which was analysed 16 weeks post-treatment. Clinical assessments included neurological exams, CSF and urine biomarkers, and 7 T MRI and magentic resonance spectroscopy (MRS). Post-mortem analysis included β-galactosidase and virus distribution, histological analysis and ganglioside content.

Untreated GM1 animals survived 8.0 ± 0.6 months while intravenous treatment increased survival to an average of 3.5 years ($n = 2$) with substantial improvements in quality of life and neurological function. Neurological abnormalities, which in untreated animals progress to the inability to stand and debilitating neurological disease by 8 months of age, were mild in all treated animals. CSF biomarkers were normalized, indicating decreased CNS cell damage in the treated animals. Urinary glycosaminoglycans decreased to normal levels in the long-term cohort. MRI and MRS showed partial preservation of the brain in treated animals, which was supported by post-mortem histological evaluation. β-Galactosidase activity was increased throughout the CNS, reaching carrier levels in much of the cerebrum and normal levels in the cerebellum, spinal cord and CSF. Ganglioside accumulation was significantly reduced by treatment. Peripheral tissues such as heart, skeletal muscle, and sciatic nerve also had normal β-galactosidase activity in treated GM1 cats. GM1 histopathology was largely corrected with treatment. There was no evidence of tumorigenesis or toxicity.

Restoration of β-galactosidase activity in the CNS and peripheral organs by intravenous gene therapy led to profound increases in lifespan and quality of life in GM1 cats. These data support the promise of intravenous gene therapy as a safe, effective treatment for GM1 gangliosidosis.

1 Scott-Ritchey Research Center, College of Veterinary Medicine, Auburn University, Auburn, AL 36849 USA
2 Department of Anatomy, Physiology, and Pharmacology, College of Veterinary Medicine, Auburn University, AL 36849 USA
3 Biology Department, Boston College, Chestnut Hill, MA 02467 USA

4   Department of Neurology, University of Massachusetts Medical School, Worcester MA 01605 USA
5   Horae Gene Therapy Center, University of Massachusetts Medical School, Worcester MA 01605 USA

[†]Present address: Department of Radiology, University of Massachusetts Medical School, Worcester, MA 01605 USA

Correspondence to: Douglas R. Martin
Scott-Ritchey Research Center, College of Veterinary Medicine
Auburn University, 1265 HC Morgan Drive, Auburn, AL 36849 USA
E-mail: martidr@auburn.edu

Introduction

GM1 gangliosidosis is a progressive neurodegenerative disease caused by a mutation of the *GLB1* gene, resulting in a deficiency of β-galactosidase (βgal, EC 3.2.1.23).[1] GM1 is a lysosomal storage disease, which as a group, represent over 50 distinct diseases.[2] In the lysosome, βgal is used to break down GM1 ganglioside and therefore a deficiency in βgal results in accumulation of GM1 ganglioside.[3] GM1, which can occur at any stage of life, is divided into three types based on age of onset: type I (infantile), type II (late infantile/juvenile) and type III (adult/chronic).[1,4] The most common forms of GM1 are infantile and juvenile, which have a more rapid disease progression than the adult onset phenotype. All forms of GM1 are characterized primarily by debilitating and progressive neurological disease, although accumulation of substrates with terminal galactose moieties occurs throughout the body.[5] Outside of palliative and supportive care, there is no effective therapy for GM1.

Animal models are useful and necessary for evaluating candidate therapeutics before initializing clinical trials. Murine[6–8] and feline[9] models of GM1 both exist and have been well characterized. The feline GM1 disease model closely resembles the type II phenotype in human patients.[10,11] While mouse models provide an invaluable resource for studying disease progression and treatment, they do not always mimic the human clinical disease phenotype. Additionally, their limited lifespans prevent long-term studies.[12] Feline brains are 50× larger than murine brains and more closely resemble the architecture and organization of the human brain.[13] Previously, both models showed recovery of βgal activity throughout the CNS after injection of adeno-associated viral (AAV) vectors into the brain parenchyma and CSF.[14–16] Widespread CNS distribution of enzyme via intraparenchymal injection is dependent on treating highly interconnected brain structures such as the deep cerebellar nuclei (DCN),[17] thalamus[14] and striatum.[18,19] In the feline model of GM1, bilateral injection of AAV into the thalamus and DCN showed a marked improvement in quality of life and lifespan, with minimal neurological symptoms.[16] While the intraparenchymal injections were successful, the risk of serious adverse events due to intracranial surgery, volume and administration rate are concerns that must be addressed for human patients.[20] Although invasive, brain parenchyma injections were the only way to treat the CNS effectively until the advent of a method to circumvent the blood–brain barrier.

AAV9, as well as other AAV serotypes, cross the blood–brain barrier and transduce neurons and glial cells throughout the CNS after systemic injection.[21–23] Systemic delivery of AAV also leads to high transduction of peripheral tissues, which is expected to benefit the global enzyme deficiency and storage accumulation in GM1. Administration of AAV9 intravenously in GM1 mice restored enzymatic activity in the cerebrum and cerebellum to 16–24% of normal, with reduction but not complete normalization of GM1 ganglioside storage. Survival of treated GM1 mice increased significantly by ~90%.[24] While these results are encouraging, the scalability of this approach to humans, with a brain size >2000 times larger than the mouse, must be tested in a larger animal. Intravenous administration of AAV9 led to expression of green fluorescent protein throughout the whole spinal cord in neonatal and adult cats,[25] indicating the applicability of intravenous administration of AAV for neurological diseases in a large animal model. Thus, with the goal of developing a minimally invasive treatment, and the promise of AAV in numerous indications, the current study treated GM1 cats intravenously with AAV9 gene therapy as a test of scale-up and potential efficacy in human clinical trials.

Materials and methods

Vectors

The AAV backbone expressing feline βgal was previously described[16] and contained a hybrid chicken β-actin (CBA) promoter, including the CMV immediate-early enhancer fused to the CBA promoter.[26] The woodchuck hepatitis virus post-transcriptional regulatory element (WPRE) was included for enhancement of gene expression, although the effects of WPRE are often vector-specific. The vector was produced by triple transfection of 293T cells with the helper plasmid (Fd6),[27] the plasmid expressing AAV9 capsid (pAR-9)[28] and the plasmid containing the feline βgal expression unit, and purified using an iodixanol density gradient. An additional virus was made using the same vector backbone but without WPRE.

Animals and injection procedure

All animal procedures were approved by the Auburn University Institutional Animal Care and Use Committee and comply with the Animal Welfare Act. Animals were group housed in a closed research colony with IACUC-approved standard runs having padded nesting boxes and resting boards. The runs were maintained on standard, IACUC-approved light/dark cycles, and

Table 1 Intravenous treatment of GM1 cats with AAV9

Group	Cat	Gender	Treatment age (months)	Treatment weight (kg)	Necropsy age (months)	CRS at necropsy
Short-term	9–1916	Female	1.5	0.5	5.3	10.0
	9–1920	Female	1.3	0.4	5.0	10.0
	9–1925	Male	1.3	0.5	5.0	10.0
	9–1933	Male	1.4	0.6	5.1	9.0
	Mean ± SD		1.4 ± 0.1	0.5 ± 0.1	5.1 ± 0.1	9.8 ± 0.4
Long-term	8–1714	Male	1.2	0.6	43.9	8.5
	8–1716	Female	1.2	0.5	40.3	8.5

CRS = clinical rating score; SD = standard deviation.

animals were provided with daily socialization, enrichment and *ad libitum* access to food and water. Animal welfare was assessed at least twice daily by colony personnel and weekly by a unit attending veterinarian representing the Division of Laboratory Animal Health.

Treatment groups for this study are detailed in Table 1. Cats diagnosed with GM1 gangliosidosis were treated with an AAV9 vector expressing feline βgal at a total dose of 1.5×10^{13} vector genomes (vg)/kg body weight. Treatment was administered to unsedated animals at 1.3 ± 0.1 months of age and ~0.5 kg body weight via a cephalic vein catheter. Injection rate was 0.3 ml/min. Vector injection was followed by ~0.5 ml of saline flush.

Animals were assessed every 2 weeks using a 10-point clinical rating score. The scale is based on neuromuscular disease severity and reflects symptom onset: 10 = normal, 9 = hind limb weakness, 8 = wide stance, 7 = ataxia, 6 = instability with occasional falling, 5 = can walk at least four steps, 4 = can stand but cannot walk, 3 = cannot stand (typical humane end point). An additional point is removed from the clinical score for onset of tremors (fine, overt) or limb spasticity (front, hind). Animals were evaluated for 16 weeks post-treatment (short-term) or until humane end point (long-term), defined as the inability to stand. The brain was divided into 6-mm coronal blocks with the right hemisphere and select peripheral tissues preserved in optimal cutting temperature (OCT) medium. All other tissues were flash frozen in liquid nitrogen and stored at –80°C or were formalin-fixed.

The number of untreated control animals for the short-term cohort was $n = 6$ (normal) or $n = 5$ (GM1). The number of untreated control animals for the long-term cohort was $n = 5$ (normal) or $n = 7$ (GM1). Since untreated GM1 cats survive to only 8 months of age, GM1 cats at ~8 months were used for long-term controls. Not all control animals were used for all analyses. The minimum number of control animals used for any given analysis was $n = 3$ or 4 (with the exception of IBA-1 expression in untreated GM1 cats, for which $n = 2$ due to technical complications with staining and availability of tissue; statistical comparisons were not performed for IBA-1 staining in untreated GM1 cats).

MRI and MRS

Animals were fully anaesthetized for MRI using a combination of intravenous ketamine (10 mg/kg) and dexmedetomidine (0.04 mg/kg) and anaesthesia was maintained using isoflurane. MRI and magnetic resonance spectroscopy (MRS) data were acquired on a 7-T MAGNETOM scanner (Siemens Healthcare). A 32-channel head coil (Nova Medical) was used for all scans. Anatomical coronal images were acquired using 3D MPRAGE (magnetization-prepared rapid gradient echo) with 0.5 mm isotropic resolution and repetition time/echo time (TR/TE) of 1910/2.5 ms, followed by 2D axial T_2 turbo spin echo images with TR/TE of 5450/12 ms and a resolution of (0.25 × 0.25 × 1) mm. Single voxel spectroscopy was then acquired using a

PRESS (point resolved spectroscopy) sequence optimized for 7 T with TE/TR = 30/5000 ms, 64 averages and a variable pulse power and optimized relaxation delays water suppression. Shimming was performed using FASTESTMAP followed by manual shimming if needed. The resulting full-width at half-maximum of unsuppressed water was typically 16 Hz. Optimization of RF pulse amplitudes and of the water suppression scheme was performed before acquiring each spectrum. The unsuppressed water signal was obtained and used for eddy current correction and for quantification of metabolites. Using high-resolution 3D MRI images, voxels were positioned in the thalamus (7 × 6 × 8 mm), parietal cortex (7 × 6 × 8 mm) and cerebellum (7 × 7 × 8 mm). MRI data were analysed with EFilm 3.2 software (Merge Healthcare, Chicago). MRS data were processed with LC model and internal water scaling (http://www.s-provencher.com/lcmodel.shtml). Representative MRS spectra from the normal, GM1 untreated and the short-term cohort with major metabolite peaks labelled are shown in Supplementary Fig. 1.

Two MRI sections, one from cerebrum and one from cerebellum, were analysed using ImageJ.[29] Separate regions of interest were drawn around the approximate anatomical region for the grey and white matter for each image. The average intensity for each region of interest was measured and the average white matter intensity was subtracted from the average grey matter intensity as a quantitative representation of brain pathology measured by MRI.

Lysosomal enzyme activity

Lysosomal enzymes were isolated from CNS tissues with three to six sections (40 μM) cut from coronal blocks stored in OCT. For peripheral tissues, 50–70 mg was taken from the flash frozen samples. Tissues were homogenized manually in 500 μl of 50 mM citrate phosphate buffer, pH 4.4 (50 mM citric acid, 50 mM Na_2HPO_4, 10 mM NaCl) containing 0.1% Trition X-100 and 0.05% BSA, followed by two freeze–thaw cycles in liquid nitrogen and centrifugation at 15 700*g* for 5 min at 4°C. The activity of βgal was measured using synthetic fluorogenic substrates as previously described.[30] CSF samples were analysed for βgal activity using 30 μl of sample and 100 μl of substrate and incubated at 37°C for 1 h. Specific activity was expressed as nmol 4 MU cleaved/mg protein/h after normalization to protein concentration determined by the Lowry method.

Distribution of βgal activity was determined via histochemical staining as previously described.[16]

Ganglioside content

As described in greater detail previously,[31] total lipids were extracted with chloroform ($CHCl_3$) and methanol (MeOH) 1:1 by volume and purified from the lyophilized brain tissue.[32–34] Neutral and acidic lipids were separated using DEAE-Sephadex (A-25;

Pharmacia Biotech) column chromatography.[35] The total lipid extract was applied to a DEAE-Sephadex column after suspension in solvent A (CHCl$_3$: CH$_3$OH: dH$_2$0, 30:60:8 by volume), which also was used to collect the neutral lipid fraction. Acidic lipids were eluted from the column with CHCl$_3$:CH$_3$OH: 0.8 mol/l Na acetate (30:60:8 by volume), dried by rotary evaporation, and then partitioned so that acidic lipids were in the lower organic phase and gangliosides were in the upper aqueous phase.[36–38] The resorcinol assay was used to measure the amount of sialic acid in the ganglioside fraction, which then was further purified with base treatment and desalting. Neutral lipids were dried by rotary evaporation and resuspended in CHCl$_3$:CH$_3$OH (2:1 by volume). Gangliosides were analysed qualitatively by HPTLC and quantitated as previously described.[31,34] Total brain ganglioside distribution was normalized to 100% and the percentage distribution was used to calculate sialic acid concentration of individual gangliosides.[33]

Biomarker analysis

Cats were sedated using dexmedetomidine (0.04 mg/kg) for CSF collection and as needed for blood collection. Blood was collected from the jugular vein and CSF was collected from the cerebellomedullary cistern. CSF samples underwent one freeze–thaw cycle before being analysed for aspartate aminotransferase (AST) and lactate dehydrogenase (LDH) concentration using a Cobas C311 chemistry analyser (Roche Hitachi). Complete blood counts and serum chemistries were conducted as previously described.[39]

Quantitative PCR

Genomic DNA was isolated from both OCT embedded tissues and fresh frozen tissues using the DNeasy blood and tissue kit (Qiagen) according to the manufacturer's protocol. Quantitative PCR was conducted using 50 ng of DNA using SsoAdvanced Universal SYBR Green Supermix (Bio-Rad) and a QuantStudio 3 real-time PCR system (ThermoFisher). Vector genomes were determined using a standard curve run with samples ranging from 1×10^8 to 1×10^2 molecules/μl from the transgene plasmid and primers for the SV40 polyadenylation site. Feline albumin was used for comparison.[40] A standard curve was created using gDNA from normal cat liver using a 150 bp sequence from the fALB primers, quantified on a NanoDrop One^c (ThermoFisher) and diluted to range from 1×10^8 to 1×10^2 molecules/μl. Primers were as follows: SV40 forward primer: AGCAATAGCCATCACAAATTTCACAA; SV40 reverse primer: CCAGACATGATAAGATACATTGATGAGT; Feline albumin forward primer: GATGGCTGATTGCTGTGAGA; Feline albumin reverse primer: CCCAGGAACCTCTGTTCATT. Results are expressed as vector genomes/cell by dividing the SV40 quantity by the albumin quantity.

Serum antibody evaluation

Serum antibody titres were determined in a similar way to a previously described protocol.[41] Briefly, 4.6×10^{12} vector genomes of an AAV9 encoding green fluorescent protein was coated onto an ELISA plate (Nunc) and incubated overnight at 4°C. Compared to the therapeutic vector expressing the feline βgal cDNA, the GFP virus produced an equivalent response in pre- and post-treatment feline serum samples from this study (data not shown). The following day, the plates were washed and blocked with 5% non-fat powdered milk in PBS for 90 min. Plates were then incubated with 2-fold serial dilutions of feline serum samples, starting either at 1:8 or 1:500. Goat anti-feline IgG: HRP (Jackson ImmunoResearch, 1:20 000) was used with tetramethylbenzidine (Pierce) for colour development.

Histopathology

Paraffin embedded tissue sections (4 μm) were stained with haematoxylin and eosin (H&E) on a Autostainer XL (Leica) and with GFAP (undiluted, Dako), IBA-1 (1:750 dilution, Biocare Medical) and Olig2 (1:200 dilution, Abcam) on a Autostainer Link 48 system (Dako), using an Envison Flex kit (Dako). After staining, the IBA-1, GFAP and Olig2 slides were scanned using Leica Scanscope at ×40 and analysed using algorithms developed in-house on Visiopharm software (Broomfield, CO, USA). Paraffin embedded tissue sections (4 μm) were stained with Luxol Fast Blue (LFB; 0.1% in 95% alcohol with acetic acid, Electron Microscopy Sciences) and differentiated with lithium carbonate (0.05%, Diagnostic Biosystems) and 70% ethanol, then counterstained with Mayer's haematoxylin (Electron Microscopy Sciences).

Urine glycosaminoglycans

Glycosaminoglycans (GAGs) in the urine were measured as previously described[39] in normal cats, GM1 untreated cats at ~8 months of age (humane end point), and both cohorts of treated GM1 cats. Data are presented as μg GAG/mg protein/dl urine.

Cell culture

Immortalized fibroblasts from either normal (NSV3) or GM1 (GM1SV3) felines[42] were maintained and studied at 37°C in Dulbecco's modified Eagle medium (4.5 g/l D-glucose, 25 mM HEPES, with L-glutamine, Thermo Fisher Scientific) supplemented with 1% (v/v) antibiotic-antimycotic (Thermo Fisher Scientific) and 10% (v/v) foetal bovine serum (Milipore Sigma) in a humidified atmosphere with 5% CO$_2$. For evaluation of the different vectors, fresh media was added to cells seeded in six-well plates with AAV added at three different concentrations (5^6, 5^5 and 5^4 vg/cell) and incubated for 24 h, followed by a change of media and incubation for an additional 3 days. The experiment was repeated three times. Cells were manually dissociated from the plates and assayed using the lysosomal enzyme activity protocol described previously.

Statistics

Statistical analyses were performed using Prism (Graphpad, La Jolla, CA USA) and Microsoft Excel (Microsoft, Redman, WA USA). Brown–Forsythe and Welch one-way ANOVA tests were used to compare all groups for statistical significance. For MRS, only spectra with Cramér–Rao minimum variance bounds of <30 were included in the analyses. Also for MRS, statistical comparisons were made between AAV-treated cats at 5 months of age and untreated controls at 6 months of age. However, comparisons with other control groups may be found in Supplementary Table 1.

Data availability

Most data are available in the main text or the Supplementary material. Any additional data that supports the findings of this manuscript are available from the corresponding author on reasonable request.

Results

Clinical data

The objective of this study was to determine the efficacy of an AAV9 vector expressing feline βgal in correcting neurological and biochemical symptoms of cats with GM1 after a single intravenous injection. Six animals were injected at ~1.3 months of age (Table 1). They were divided into two cohorts; the short-term group was necropsied at 5.1±0.1 months of age (16-weeks post-
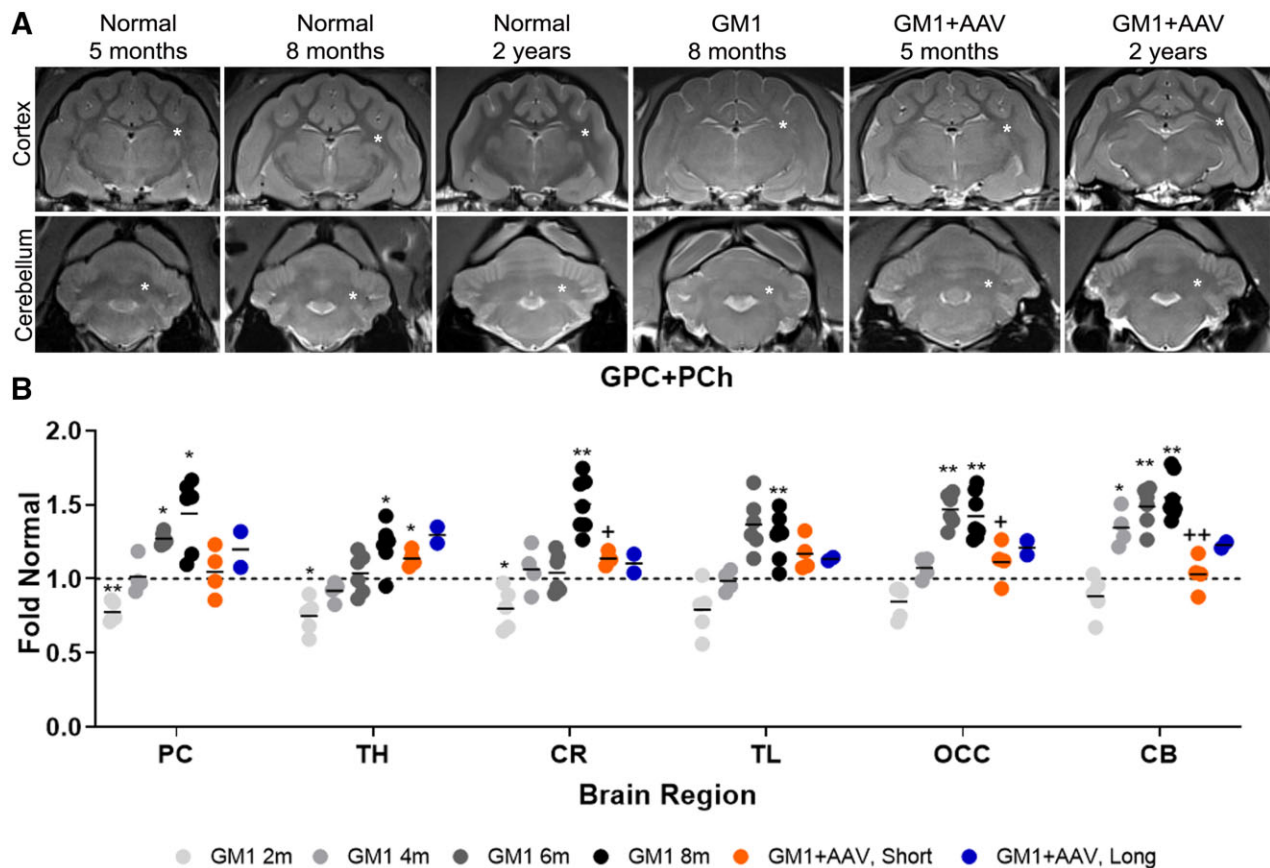
Figure 1 MRI and MRS evaluation of GM1 + AAV animals. (**A**) In normal cats, white matter is hypointense to grey matter on T_2-weighted images. Untreated GM1 animals have isointense grey and white matter, with atrophy indicated by increased CSF (bright white) around and within the brain. At both time points (5 months and 2 years), treated animals had normalized grey: white matter intensities and minimal changes to CSF levels. Similar regions of white matter indicated with white asterisk on each image. (**B**) Glycerophosphocholine and phosphocholine (GPC + PCh) was measured via MRS in six voxels: parietal cortex (PC), thalamus (TH), corona radiata (CR), temporal lobe (TL), occipital cortex (OCC) and cerebellum (CB). Scans were performed at 2, 4, 6 and 8 months of age in untreated GM1 cats, 5 months in the short-term cohort (GM1 + AAV, Short), and 2 years in the long-term group (GM1 + AAV, Long). Measurements are standardized to the appropriate age-matched normal controls and are represented as fold normal. The solid horizontal lines indicate the means for the groups. The dashed horizontal line represents levels in normal animals. $^*P < 0.05$ and $^{**}P < 0.005$ versus age-matched normal and $^+P < 0.05$ and $^{++}P < 0.005$ versus age-matched untreated GM1. Statistical analyses were not performed for the long-term cohort ($n = 2$).

treatment) and the long-term group was followed to humane end point. Neurological symptoms were tracked with a 10-point clinical rating score (CRS), detailed in the 'Materials and methods' section. Untreated animals progress through disease symptoms beginning with hind limb weakness and fine tremors to ataxia and overt body tremors. Humane end point is reached at ~8 months of age. In the short-term cohort, three of the four animals had no clinical symptoms by the predetermined end point at ~5 months of age. One short-term animal had hind limb weakness, the first sign of clinical disease (Table 1). In comparison, untreated GM1 cats at ~5 months of age exhibit hind limb weakness, wide stance, ataxia and overt body tremors. Both animals in the long-term cohort exhibited a mild hind limb weakness and slight wide based stance from ~3 months of age until euthanasia at 40.3 and 43.9 months (Supplementary Fig. 2). Long-term animals were humanely euthanized due to weight loss, possibly due to pancreatitis, rather than the typical neurological end point of this model. The long-term cohort lived an average of 5.3 times longer than untreated GM1 animals (Table 1).

MRI/MRS

Brain architecture was evaluated using an ultra-high field (7 T) T_2-weighted MRI (Fig. 1A). In untreated GM1 animals at or near the

humane end point, the grey and white matter were isointense (of the same degree of darkness), due to demyelination in the white matter and increased GM1 storage in grey matter in both the cerebral cortex and cerebellum. Additionally, there was an increase in CSF surrounding the brain and within the ventricles due to cortical atrophy. Sixteen weeks after intravenous injection of GM1 cats (5 months of age), white matter remained hypointense to grey matter, as in normal cats, in both the cerebral cortex and cerebellum (Supplementary Fig. 3A and B). There was a minor increase in CSF (brain atrophy) in the short-term cohort. Two years post-intravenous injection, the grey–white matter boundaries of GM1 cats and overall brain architecture were partially preserved in comparison to end point untreated GM1 animals (Fig. 1A and Supplementary Fig. 3A and B).

MRS of the parietal cortex, thalamus, corona radiata, temporal lobe, occipital cortex and cerebellum corroborated the MRI images showing demyelination[43] in untreated GM1 animals. Commonly used as indicators of demyelination, glycerophosphocholine (GPC) and phosphocholine (PCh) increase with cell turnover due to their role in membrane synthesis and degradation.[44] In all voxels of untreated GM1 animals, GPC + PCh increased with disease progression (Fig. 1B and Supplementary Fig. 4). Intravenous treatment decreased the levels of GPC + PCh in both the short- and long-term cohorts.
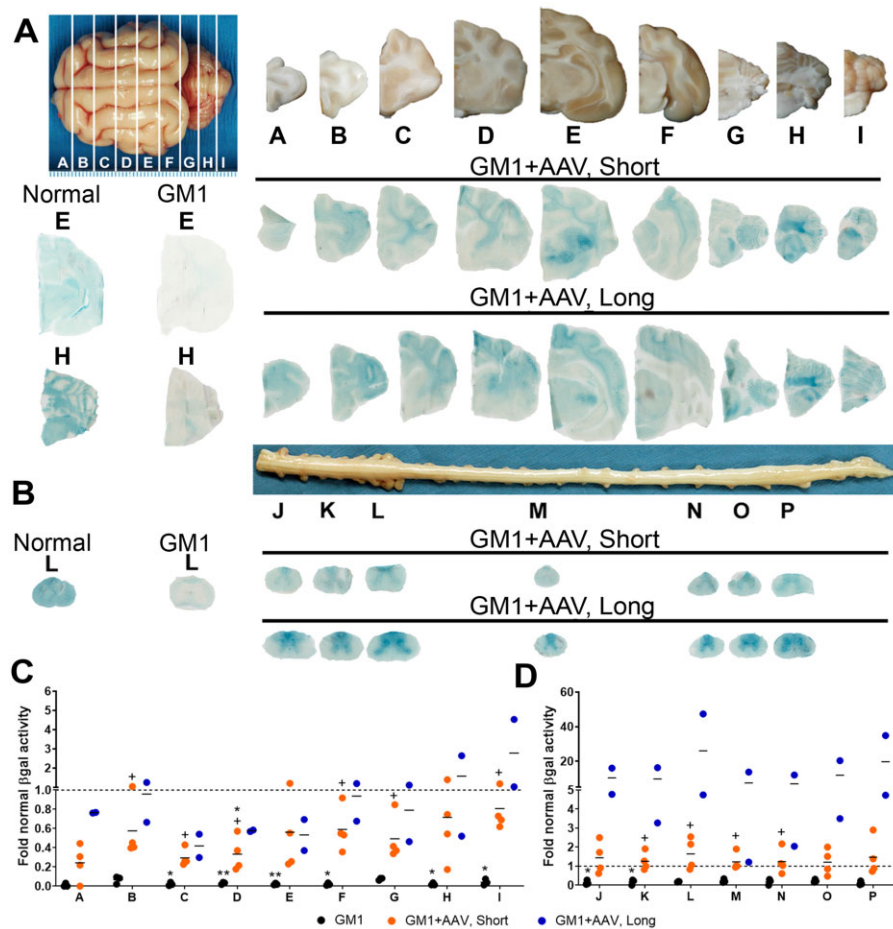
Figure 2 Activity and biodistribution of βgal in GM1 + AAV animals. (**A**) *Top left*: Gross image of the feline brain with letters indicating the 6 mm blocks used in analysis. *Top right*: Gross images of the right hemisphere of each brain block, which was used for measuring βgal activity and distribution in treated cats (blue stain). Also shown are representative sections from normal and GM1 control animals. (**B**) Regions of the spinal cord tested for βgal activity. βGal activity in homogenate from each brain block (**C**) and spinal cord segment (**D**) expressed as fold of normal activity. Graphs show activity from untreated GM1 animals at humane end point (GM1), the short-term cohort (GM1 + AAV, Short), and the long-term cohort (GM1 + AAV, Long). Dashed horizontal line represents normal activity and the horizontal lines for each measurement represents the mean for the group. *$P < 0.05$ versus normal cats and $^{+}P < 0.05$ versus untreated GM1 cats. Statistical analyses were not performed for the long-term cohort ($n = 2$).

Preservation of GPC + PCh levels in treated GM1 animals was apparent in several voxels of short-term animals. Mean levels of GPC + PCh in treated cats from the long-term cohort were below that of untreated cats in almost every voxel.

Additional metabolites studied included myoinositol (glial marker[45]), N-acetyl aspartate with N-acetyl aspartyl glutamate (neuronal marker[46]), creatine with phosphocreatine (metabolism markers[47]) and glutamate with its precursor glutamine (neurotransmitter[48]) (Supplementary Figs 5–8). By the humane end point in untreated GM1 cats, there was an elevation in myoinositol in the thalamus, with significant elevation in the corona radiata and cerebellum (Supplementary Fig. 5). Treatment led to partial preservation of myoinositol levels in these regions in most animals, with normal levels in one cat of the long-term cohort. Creatine with phosphocreatine were also elevated in end point GM1 animals (Supplementary Fig. 6). Intravenous gene therapy improved levels of both metabolites in the cerebellum in short- and long-term cohorts. N-acetyl aspartate and N-acetyl aspartyl glutamate (Supplementary Fig. 7) demonstrated a significant decrease with age in the cerebellum, which was partially corrected after treatment. No clear trend existed for glutamate with glutamine (Supplementary Fig. 8).

Biodistribution

Intravenous injection of AAV9 produced a broadly distributed increase of βgal activity throughout the entire CNS of cats in short- and long-term cohorts (Fig. 2). βGal activity was widely distributed through the brain (blocks A–I), including the thalamus and cerebellum, as shown by X-gal staining (Fig. 2A). Normal or above-normal enzyme activity was measured in the cerebellum (blocks H and I) of the long-term cohort. βGal activity in the brain of the long-term cohort ranged from 0.4- to 2.8-fold normal and in the short-term cohort ranged from 0.2- to 0.8-fold normal (Fig. 2C). Similarly, βgal activity was present throughout the entire spinal cords of all treated animals and primarily localized in the grey matter (Fig. 2B). In the spinal cored βgal levels ranged from 7.1- to 26.0-fold above normal in the long-term cohort and 1.2- to 1.6-fold above normal in the short-term cohort (Fig. 2D). Although variability existed in both cohorts, all animals had similar trends in enzyme activity. Additionally, the high standard deviation in the short-term treatment group can be attributed to two animals having a lower overall activity, although relative βgal distribution was similar among all animals in the cohort.

Vector was well distributed, although in low levels, throughout the brain in both the short- and long-term cohorts (Supplementary
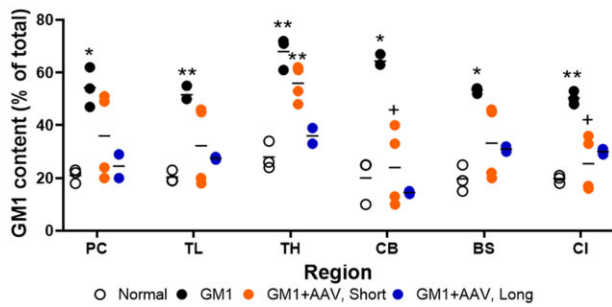
Figure 3 GM1 ganglioside content decreases following AAV gene therapy. GM1 ganglioside content in the CNS of normal, treated and untreated GM1 animals. Data were determined from densitometric scanning of HPTLC plates and is shown as a percentage of total ganglioside content. The horizontal lines indicate the mean of the measurements. BS = brainstem; CB = cerebellum; CI = cervical intumescence of spinal cord; PC = parietal cortex; TH = thalamus; TL = temporal lobe. $^*P < 0.05$, $^{**}P < 0.005$ versus normal; $^+P < 0.05$, $^{++}P < 0.005$ versus untreated GM1. Statistical analyses were not performed for the long-term cohort ($n = 2$).

Fig. 9A). Similar levels of vector genomes were detected in most brain blocks within each cohort, with highest levels in the frontal cortex (block A). Evaluation of individual brain structures revealed similar levels of AAV in each, with slight but significant elevations in the parietal cortex, thalamus, occipital cortex and brainstem and near-background levels of vector in the caudate nucleus and DCN for the short-term cohort. The two cats in the long-term cohort had slightly elevated levels in the temporal lobe, occipital cortex and brainstem (Supplementary Fig. 9B). AAV also was detected in the spinal cord at similar levels in both cohorts, with near-background values in the rostral cervical region and higher values in the cervical intumescence, thoracic and lumbar regions (Supplementary Fig. 9C). In peripheral tissues of short-term cohort animals, the highest levels of vector were measured in heart, which had 5.5 times as much vector as liver and 30.3 times as much vector as spleen. In the long-term cohort animals, there was 7.2 times as much vector in the heart as the liver and 14 times as much vector as in the spleen (Supplementary Fig. 9D). In comparison with the brain section having the highest vector content, the heart had 198.7 times more vector in the short-term cohort and 36.5 times as much vector in the long-term cohort. Additionally, relative to the spinal cord block with the highest vector content, there was 130.4 times more vector in the heart of the short-term cohort and 93.1 times more vector in the heart of the long-term cohort.

Ganglioside content

GM1 ganglioside was measured in the parietal cortex, temporal lobe, thalamus, cerebellum, brainstem and cervical intumescence of the spinal cord in normal, treated and untreated GM1 animals (Fig. 3). Ganglioside levels in untreated GM1 cats were significantly elevated in all regions, ranging from 2.4 to 3.2 times normal. Sixteen weeks after treatment, mean GM1 ganglioside levels were reduced, with significant decreases to near-normal levels in the cerebellum and cervical intumescence of the spinal cord. The long-term cohort had significant decreases in GM1 ganglioside in all regions, with normalized levels in the parietal cortex, thalamus and cerebellum.

CSF biomarkers

βGal activity in the CSF was elevated above untreated animals in both cohorts of treated animals (Fig. 4A). βGal levels were 0.4 ± 0.1-fold of normal in the short-term cohort and 8.5 ± 6.4-fold above
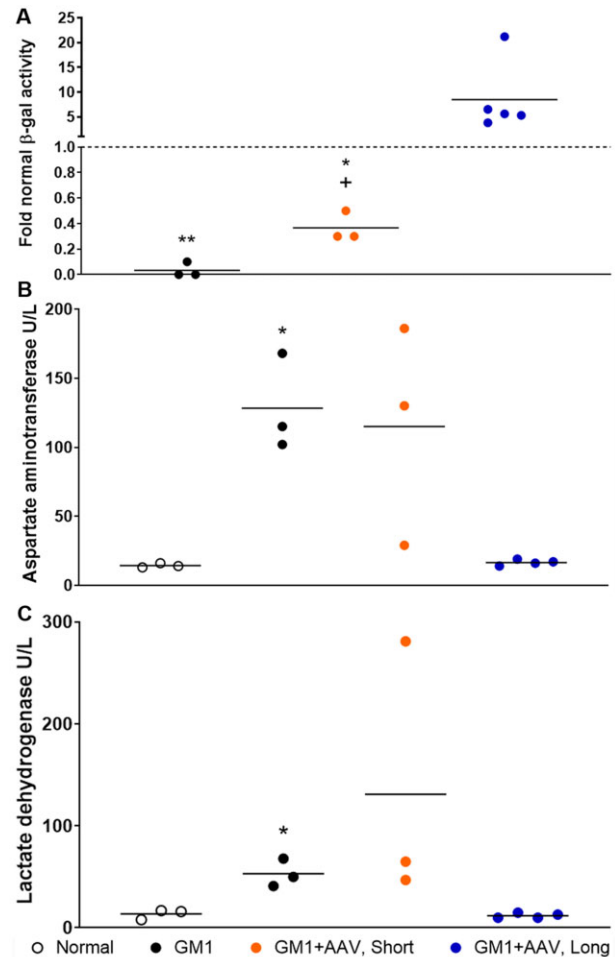

Figure 4 Long-term normalization of CSF biomarkers. (**A**) βGal activity in CSF of untreated animals (GM1), the short-term cohort (GM1 + AAV, Short, $n = 3$) and the long-term cohort (GM1 + AAV, Long, $n = 5$). The long-term samples were collected between 17.8 and 40.3 months of age. Data are represented as fold normal activity with the mean represented as a horizontal line. The dashed horizontal line indicates normal activity. CSF biomarker levels for aspartate aminotransferase (AST, **B**) and LDH (**C**) in normal, untreated GM1 and treated GM1 animals. The short-term cohort represents samples taken at the experimental end point (~ 5 months of age) and the long-term cohort represents two separate measurements per animal at two different time points, between 17.8 and 30.4 months of age. The horizontal line indicates the mean. $^*P < 0.05$ and $^{**}P < 0.005$ versus normal; $^+P < 0.05$ versus untreated GM1 animals. Statistical analyses were not performed for the long-term cohort ($n = 2$).

normal in the long-term cohort. CSF markers of cellular damage correlate with disease progression in GM1.[39] Aspartate aminotransferase (AST, Fig. 4B) and LDH (Fig. 4C) were elevated in untreated GM1 animals. Both AST and LDH were normalized in two animals of the short-term cohort (9–1916 and 9–1933), but not in the other animals (9–1920 and 9–1925). Normalization of AST and LDH levels occurred in the short-term animals with the highest levels of βgal activity in the CNS (Fig. 4). The long-term cohort showed normal levels of AST and LDH ~ 2 years after treatment.

Evaluation of immune response/adverse effects of treatment

Following treatment, all animals had antibodies to AAV9 at serum dilutions ranging from 1:1000 to 1:32 000. In the treated animals
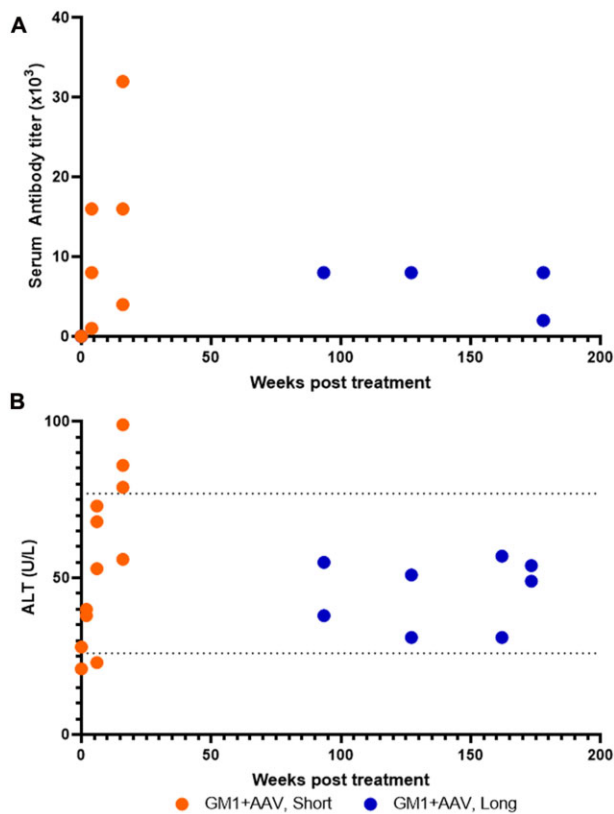
Figure 5 Serum responses to AAV gene therapy. (**A**) All treated animals had elevated serum antibody titres against AAV9 following treatment. In the long-term cohort, the concentration of antibodies decreased over time. The long-term cohort had the same antibody titre at 93 and 127 weeks post-treatment and are therefore represented as a single symbol. (**B**) Alanine aminotransferase (ALT) levels in serum increased following intravenous administration of AAV, although they were only slightly elevated above the normal reference range for cats. ALT levels decreased to normal over time, without glucocorticoid or additional treatment. The dotted lines indicate the normal reference range.

followed long-term, serum titres remained stable at or below 1:8000 for the duration of the experiment (Fig. 5A). The presence of pre-existing antibodies to AAV9 was evaluated in four of the six treated animals (pretreatment serum was not available for two cats) as well as 15 related animals (parents or siblings of treated cats). In all 19 animals, antibodies to AAV9 were undetectable at a 1:8 dilution of serum or higher (data not shown).

Alanine aminotransferase (ALT), a marker of liver insult attributed to T-cell responses to the AAV capsid,[49] increased from baseline a few months after treatment to levels slightly exceeding the reference range. However, ALT was within the reference range for cats followed long-term, without the use of glucocorticoids to reduce ALT (Fig. 5B).

Histological examination for evidence of an inflammatory or other toxic response was completed on tissue from treated animals, including eight brain and seven spinal cord blocks, heart, lung, liver, skeletal muscle, spleen, pancreas, stomach, small intestine, colon, cecum, kidney, adrenal gland, oesophagus and trachea. Evidence of inflammation or toxicity was minimal and sporadic in treated animals (Supplementary Table 2).

Histology

Untreated GM1 cats have widespread neurodegeneration in tissue sections. For example, neurons distended with foamy, vacuolated

storage are prevalent in the thalamus, cerebellum (Purkinje cells), spinal cord and numerous other sites of the CNS (Fig. 6A). Gliosis is noted throughout the cerebrum, and the cerebellum is characterized by multifocal perivascular cuffing. White matter tracts have small, clear vacuoles with swollen axons, especially in the cerebellum, and occasional evidence of necrosis is apparent at the humane end point. In treated GM1 cats, white matter tracts were within normal limits in all regions of all cats, with the exception of one animal (9–1925) that had minimal lesions to include rare spheroids and gliosis in the frontal and occipital lobes and in the cerebellum. The cerebral cortex grey matter of GM1 cats treated long-term was within normal limits or had scattered neurons with mild storage. Storage was present in the brainstem, DCN and Purkinje neurons of cats in the long-term cohort, with gliosis in some regions. Thalamic histology ranged from normal to mild/moderate storage in many neurons, with marked storage in some neurons. In the short-term group, cortical grey matter was within normal limits in two of the animals (9–1916, 9–1933, which had the highest levels of βgal activity in this cohort). In the remaining two animals treated short-term, moderate storage was apparent in neurons of all cortical layers. All cats of the short-term group had moderate storage in brainstem neurons, although it was less common in the two animals with the highest βgal activity (9–1916, 9–1933). Storage also was detected in the DCN and some Purkinje neurons in the animals with the lowest βgal activity. Thalamic neurons were primarily normal in two cats, while the remaining two cats had neurons with mild/moderate storage. Minimal residual βgal activity is present in the CNS of untreated GM1 animals, as indicated by lack of blue staining with X-gal (pH 4.2–4.5). An impressive increase in βgal activity was present throughout the CNS of animals in the short-term cohort, with particularly intense staining in thalamic neurons and Purkinje cells of the cerebellum. Moderate increases in X-gal staining were present throughout the CNS of the long-term animals. In general, areas of increased βgal activity overlapped with even mild correction of histopathology, indicating a decrease in storage.

Ionized calcium binding adaptor molecule 1 (IBA-1), a microglia marker, was increased throughout the brain of untreated GM1 animals, with statistical significance reached in the thalamus, cerebellar folia, DCN and brainstem (Fig. 6B). Both treatment cohorts trended towards normalization throughout the brain, with significance reached in the parietal cortex, cerebellar folia and DCN of the short-term cohort. Glial fibrillary acidic protein (GFAP), an astrocyte marker, was elevated in all brain regions in untreated GM1 animals (Fig. 6C). In the short-term cohort, there was a significant decrease in GFAP staining compared to untreated GM1 animals in the parietal cortex, thalamus, hippocampus, temporal lobe, occipital cortex, cerebellar folia and DCN. The long-term cohort had significantly less GFAP staining in the parietal cortex, cerebellar folia, DCN and brainstem in comparison to untreated animals. There were limited changes in either untreated GM1 animals or treated animals in oligodendrocytes, as assessed with an Olig2 antibody (Supplementary Fig. 10B). Images of these stains can be found in Supplementary Fig. 10A.

LFB, a stain used to identify myelin in nervous tissue, was decreased in untreated GM1 animals relative to normal controls (Supplementary Fig. 11). Partial normalization of the LFB levels occurred in both treated cohorts. Maintenance of white matter as shown by LFB staining agrees with and supports the MRI findings in Fig. 1A.

Peripheral disease

Since storage also occurs outside of the CNS in GM1, it is imperative to also assess the status of peripheral tissues when
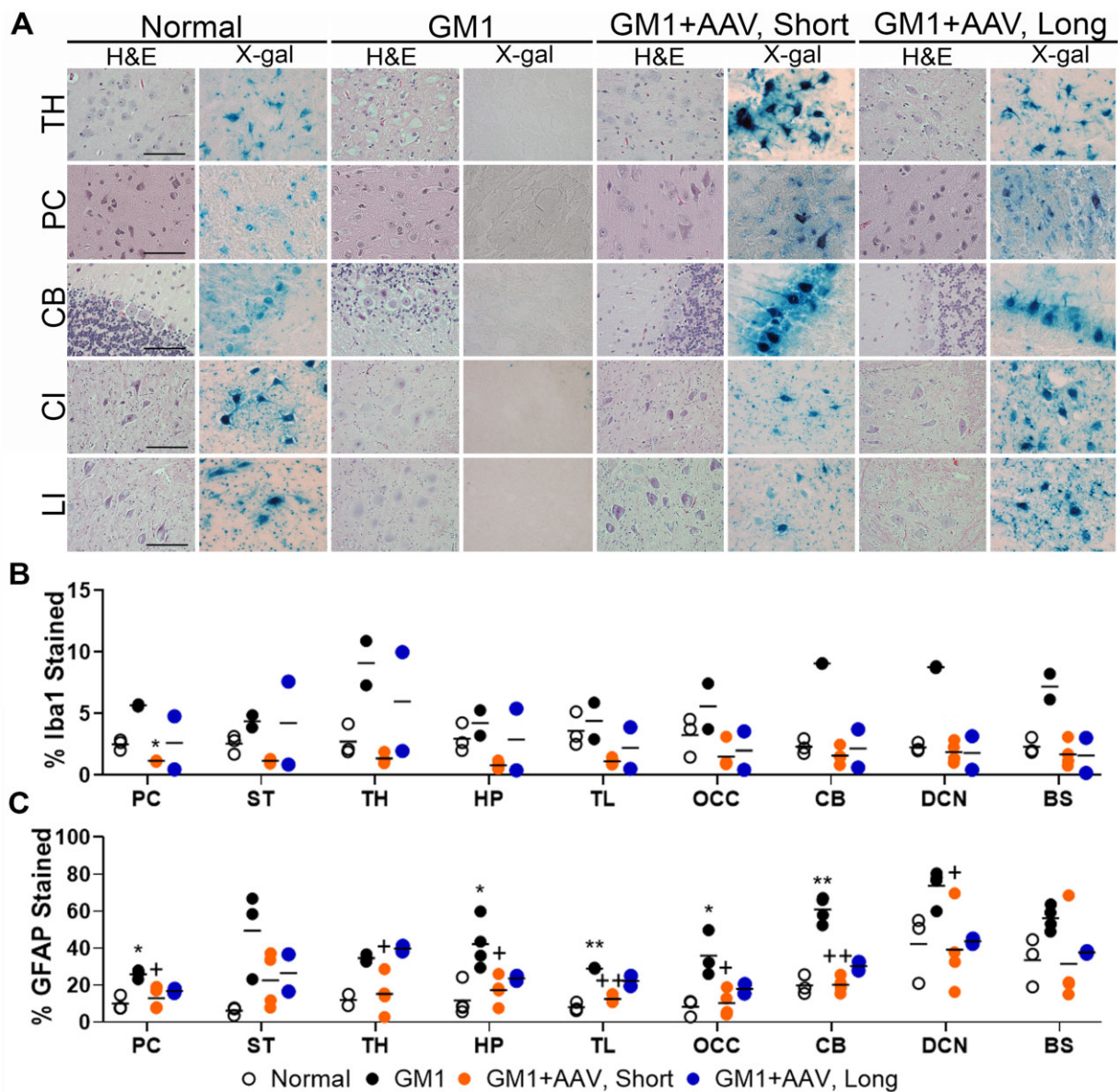
Figure 6 CNS histopathology demonstrates short- and long-term correction. (A) GM1 cats had pronounced neuronal pathology in the thalamus (TH), parietal cortex (PC), cerebellar folia (CB), cervical intumescence (CI) and lumbar intumescence (LI) of the spinal cord. Neuronal morphology was normalized in both the short-term (GM1 + AAV, Short) and long-term (GM1 + AAV, Long) cohorts. After staining with X-gal, βgal activity (blue) was seen in similar cell populations of the treated animals and normal animals. For thalamus and cerebellar folia, images were taken at ×20 magnification and scale bars = 100 μm. For cervical intumescence and lumbar intumescence, images were taken at ×40 magnification and scale bars = 50 μm. Slides stained with IBA-1 (B) and GFAP (C) were quantified for percentage of area stained in the parietal cortex (PC), striatum (ST), thalamus (TH), hippocampus (HP), temporal lobe (TL), occipital cortex (OCC), cerebellum (CB), deep cerebellar nuclei (DCN) and brainstem (BS). Horizontal bars indicate group mean. See also Supplementary Fig. 10A for representative images. *$P < 0.05$ versus normal and +$P < 0.05$ versus untreated GM1. Statistical analyses were not performed for the long-term cohort ($n = 2$) or for the GM1 cohort stained with IBA1 ($n = 2$).

determining efficacy of treatment. Normal levels of βgal activity were achieved in the sciatic nerve, heart, skeletal muscle and pituitary gland of both treated cohorts (Fig. 7A). In the long-term cohort, βgal activity was normalized in liver, spleen and adrenal gland. In untreated GM1 cats, hepatocytes were markedly expanded by enlarged, finely vacuolated foamy cytoplasm (Fig. 7B). Two cats of the short-term cohort (9–1916, shown, and 9–1933) had normal hepatocyte morphology with no storage, and the other two (9–1920 and 9–1925) had hepatocytes with mild evidence of storage. Liver histology was largely normal in both cats of the long-term treatment group, with only scant numbers of hepatocytes showing slight cytoplasmic vacuoles.

In addition to GM1 ganglioside, glycosaminoglycans are cleaved by βgal and are subsequently excreted in the urine. Untreated GM1 cats have significantly elevated amounts of urinary GAGs[39] (Fig. 7C), while GAG levels were significantly normalized in the long-term cohort. The short-term cohort displayed significantly elevated GAG levels, despite their improved phenotype. The reason for increased urinary GAG levels in GM1 cats treated for 16 weeks is yet to be determined.

Comparison of clinical vector design *in vitro*

Regulatory concerns about the WPRE led us to remove it from the clinical trial vector (https://clinicaltrials.gov/ Identifier
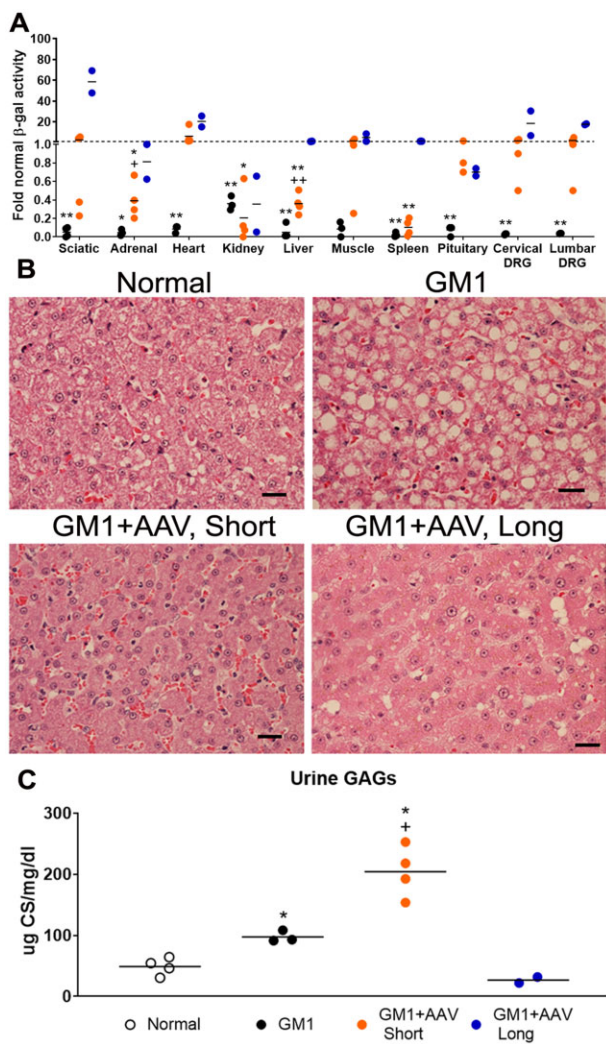
Figure 7 Correction of peripheral disease after AAV treatment. (**A**) βGal activity was measured in various peripheral organs in untreated (GM1), short-term treated (GM1 + AAV, Short), and long-term treated (GM1 + AAV, Long) animals. Data are presented as fold normal activity and the dashed horizontal line at one indicates normal activity. (**B**) Representative images of livers stained with H&E, showing accumulation of storage in the cytoplasm of hepatocytes from untreated GM1 animals. After treatment, liver histology is fully or partially preserved. (**C**) Concentration of urinary glycosaminoglycans (GAGs) were determined using a colorimetric assay. Chondroitin sulphate (CS) was used to establish the standard curve. Results are expressed as μg of GAG per mg of creatinine/dl of urine. *$P < 0.05$ versus normal and +$P < 0.05$ versus untreated GM1. Statistical analyses were not performed for the long-term cohort ($n = 2$).

NCT03952637). Because GM1 cats in the current study were treated with a vector that contained WPRE, it was important to compare βgal expression from an AAV9 vector using the same backbone but without WPRE. Tested in immortalized GM1 feline fibroblasts, βgal expression was not significantly different between vectors with or without WPRE (Supplementary Fig. 12).

Discussion

Numerous preclinical and clinical studies have demonstrated the safety and efficacy of AAV gene therapy, and the US Food & Drug Administration recently approved the first AAV vectors to treat *RPE65*-related blindness (Leber's congenital amaurosis)[50] and

spinal muscular atrophy.[51] Retinal pathology caused by *RPE65* deficiency is corrected by a direct injection of the approved AAV2 vector and spinal muscular atrophy is corrected by systemic administration of AAV9. Similarly, in previous studies, we showed that direct injection of the brain with AAV1 or AAVrh8 vectors produced profound, long-term correction of GM1 biochemically and clinically.[16,39] While untreated GM1 cats lived to 8.0 ± 0.6 months of age, those treated by intracranial AAV injection have survived an average of 5.2 years, with two treated cats still alive at >10 years of age. The efficacy of intracranial AAV treatment in the feline GM1 model is clear, but a less invasive method of treating children with severe brain disease is a critical need for widespread clinical translation.

The efficient, selective blockade that the blood–brain barrier poses was a major obstacle to the treatment of CNS disorders by intravascular routes, until certain brain-penetrant AAV variants, such as AAV9, were reported.[22,23,52] In addition to minimizing invasiveness, intravenous injection of appropriate serotypes uses the extensive vasculature of the brain as a near-global distribution network. For example, each brain neuron is estimated to be within a few micrometres of a capillary,[53] providing a built-in means of treating neurologic disorders through the bloodstream. The current study demonstrated the efficacy of intravenous delivery of AAV9 in a feline model of GM1 gangliosidosis. The widespread CNS deterioration of feline GM1 results in the inability to walk (humane end point) at ~8 months of age. Systemic infusion of AAV9 encoding feline βgal changed the course of disease progression in all treated animals, which had mild hind limb weakness and a slightly wide based stance but did not progress to more severe neurological symptoms even at ~3.5 years of age. Although intracranial injection led to a mean survival that was ~50% longer than in the current study, the two intravenous-treated cats lived to 3.4 and 3.7 years of age, substantially longer than or equivalent to, 4 of 11 cats treated intracranially (1.5, 2.1, 2.4 and 3.8 years).[16,39] Amelioration of clinical neurological disease was profound with either intravenous or intracranial treatment but, due to concerns regarding surgical risk, it has been difficult to translate the intracranial approach into clinical trials. However, partly on the basis of the results of the current study, intravenous gene therapy is under evaluation currently in GM1 children (https://clinicaltrials.gov/ Identifier NCT03952637).

MRI showed degradation of the brain architecture in untreated GM1 animals, similar to what has been previously reported in human patients.[54,55] AAV-treated animals maintained normal relative intensities of the grey matter and white matter. Additionally, brain atrophy in both the short- and long-term groups was minimal. The normalization of choline metabolites, such as GPC + PCh, is likely to indicate preservation of myelin integrity[44] and agrees with the maintenance of normal white matter appearance on anatomical MRI scans. GPC + PCh levels were normalized in many brain regions of AAV-treated cats, particularly in the corona radiata, occipital cortex and cerebellum. Additional biomarkers of disease progression, such as AST and LDH levels in the CSF, were normalized in the long-term cohort but not in the short-term cohort. While there was large disparity of AST and LDH levels as well as in urine GAG levels in the short-term cohort, it is possible that complete normalization requires longer than the predetermined 16-week follow-up for this group.

The widespread distribution of βgal activity throughout the CNS was the desired outcome of intravenous delivery, which is now possible due to a new generation of brain penetrating capsids and has advantages compared to other delivery routes. Both CSF and intracranial injections are relatively invasive compared to intravenous delivery. Intra-parenchymal injections can lead to high levels of transduction and gene expression immediately surrounding the injection site,[56,57] which may cause neurotoxicity.[58]

Although high levels of βgal activity were noted in the intravenous-treated animals, particularly in the spinal cord, no evidence of toxicity was noted either in neurological assessment or histologically. βGal activity was distributed throughout the periphery, an important consideration for whole-body protein deficiencies such as storage diseases and thus another advantage of the intravenous approach.

The many benefits of intravenous delivery should be balanced by potential disadvantages, such as a susceptibility to failure or toxicity from pre-existing serum antibodies. Recently it has been hypothesized that the tragic death of Jesse Gelsinger in 1999 resulted from pre-existing antibodies to adenovirus type 5 (Ad5), a vector under investigation for intravascular gene therapy of ornithine transcarbamylase deficiency. Enhanced transduction and activation of dendritic cells by pre-existing anti-Ad5 (hexon) antibodies are proposed to have contributed to a fatal inflammatory response to the high-dose Ad5 vector,[59] and similar concerns exist for AAV.[60] With the recent deaths of three patients with myotubular myopathy after intravenous gene therapy with a high dose of AAV8, it is crucial to understand the mechanisms of AAV vector toxicity, whether immune-mediated or otherwise.[61] However, it is important to note that even patients with pre-existing serum antibodies may be treatable by intravenous gene therapy. For example, IgG-degrading enzymes (IdeS or IdeZ) are reported to rescue intravenous gene transfer from neutralizing antibodies against AAV8 or AAV9 safely in mice and non-human primates.[62,63] Also, immunoadsorption of anti-AAV9 antibodies in rat plasma restored, partially or completely, the ability of AAV9 to transduce heart, liver and skeletal muscle.[64] In the current study, serum antibodies to AAV9 were absent in all untreated cats but did develop after treatment, as expected. An important question remains whether a single dose of AAV will be sufficient for the lifetime of the patient, and if not, whether retreatment is possible in the face of an immune response to the vector. Although depletion of existing anti-AAV antibodies through methods such as those described before may enable retreatment, another strategy is to prevent antibody formation by ablating B-cells with immune modulators such as Rituximab and Sirolimus before administration of AAV[65] (also see ClinicalTrials.gov Identifier NCT02240407). Patients who do not develop anti-AAV antibodies initially may be more suitable for retreatment using the same AAV vector.

Although antibodies to feline βgal were not evaluated in the current study, the wild-type enzyme produced by the AAV is 99.8% homologous to the endogenous mutant enzyme, which is expressed at normal levels in GM1 cats.[42] Also, the yield of feline βgal from purification methods is unusually low,[66] making it technically challenging to produce the appropriate target protein for immunoassays. Administration of AAV led to transient increases in serum ALT, often used as an indicator of T-cell response to the treatment.[49] However, samples from treated cats were not preserved for ELISpot, which can only be performed by treating further animals. Because of animal use considerations and the ongoing human clinical trial (https://clinicaltrials.gov/ Identifier NCT03952637), we decided that treating more animals was unjustified. Also, histopathological evaluation of numerous CNS and peripheral tissues found no clear evidence of cellular infiltrates in treated animals.

An important finding of the current study is the degree of βgal restoration in CNS neurons after systemic delivery of the AAV9 vector. While intravenous delivery of AAV9 beyond the neonatal period in mice is reported to transduce brain glia primarily,[23] neurons of the thalamus, cerebellum and other regions expressed high levels of βgal. Cats were treated at 1.2–1.5 months of age, a time at which the blood–brain barrier is intact, at least by measuring the quotient of albumin in the CSF versus serum. The albumin

quotient (Q_A) is a standard method for determining blood–brain barrier integrity[67] and reaches adult levels in cats between 0.9 and 1.4 months of age (unpublished data). We expect that therapeutic effect in the current study resulted from several mechanisms, including direct transduction of neurons, cross-correction of neighbouring cells with βgal via diffusion or CSF flow in perivascular spaces and axonal transport of βgal or even vector-encoded mRNA to distal sites.[68] While current analyses do not permit us to quantify the contribution of each mechanism to overall efficacy, very low vector levels in certain brain regions such as caudate nucleus suggest that cross-correction or axonal transport of βgal from distal sites plays an important role in therapeutic success. Similar results showing higher vector levels in the caudal brain, brainstem and spinal cord have been reported in several large animals including cats, cynomolgus macaques and pigs.[25,69] Broad transduction of numerous cell and tissue types is not restricted to cats. For example, intravenous injection of an AAV9-GFP construct in non-human primates led to the transduction of neurons, glial cells and motor neurons in the spinal cord, as well as skeletal muscles and peripheral organs.[69,70] Systemic delivery of AAV9 in this study effectively treated neurons in deep brain structures such as the thalamus, an advantage over CSF delivery routes published so far in large animals.

While CSF is a very effective medium for AAV transduction of cerebral cortex and other CNS regions such as spinal cord,[71–75] to date its use for treating deep brain structures in large animals is an open question.[76] For example, studies of AAV delivery through the lateral ventricles or cisterna magna have reported transduction of thalamic neurons, but the published micrographs show an exceedingly small area of the thalamus, suggesting that only a single nucleus was transduced.[77] The thalamus is a large structure, ~4 cm long in humans and 1.2 cm long in cats. Micrographs of a single, small region of the thalamus or other deep brain structures are generally ~0.5 × 0.5 mm (width × height) and are derived from a tissue section of 4–6 μm thickness, so they simply do not provide a large enough sample to reliably estimate overall transduction. When gross images of CSF-mediated vector delivery are included, they indeed demonstrate that one or two thalamic nuclei are transduced while most of the thalamus remains untreated.[78,79] Other studies report transduction of 'rare neuronal and glial cells' in a single nucleus of the thalamus,[80] which is consistent with our own results of AAV delivery through the lateral ventricles or cisterna magna in a separate feline model of lysosomal storage disease (unpublished data). Similarly, only the portion of the hypothalamus directly exposed to the third ventricle apparently was transduced after cisterna magna injection of AAV in dogs.[81] Although such results could be capsid-, construct- or species-specific, the published studies mentioned previously included three AAV serotypes (AAV1, AAV2-HBKO and AAV9) with single stranded or self-complementary backbones used in cats, dogs, pigs or non-human primates, all with little evidence of widespread transduction of deep brain structures through the CSF. Other reports of cisterna magna-mediated AAV treatment in feline models of lysosomal storage diseases demonstrate convincing efficacy in the cerebral cortex and cerebellum but show low-level transduction of deep brain structures,[82] or do not address them.[83] In the current study, broad treatment of the thalamus was achieved by intravenous delivery of AAV9 at a relatively modest dose (Fig. 2) and represents a potential advantage over CSF delivery to treat global brain disorders. It is possible that a combination of CSF and intravenous delivery routes will maximize the advantages of each strategy to achieve optimal therapeutic results.

New AAV serotypes have demonstrated outstanding, global brain transduction including deep brain structures after intravenous or CSF delivery in mice,[84] but such novel capsids have either

undergone limited testing in large animals[85] or, in the case of AAV-PHP.B given by cisterna magna injection in non-human primates, show 'a very low level of transduction in several subcortical areas including the caudate, putamen, hypothalamus, substantia nigra and medulla'.[86] Similar reports confirm that the high efficiency of PHP.B in mice does not translate to the brain of non-human primates following intravenous administration.[87,88] Although CSF-based methods of treating deep brain structures in large animals may not yet be optimized, transformative results have been achieved in certain disorders, such as the canine model of Krabbe disease. Affected dogs treated presymptomatically by cisterna magna delivery of a high AAV9 dose (1×10^{14} vg) were, at the time of publication, neurologically normal at an average age eight times older than the lifespan of untreated dogs. Even with this strong degree of efficacy, it is interesting that neither AAV vg nor galactosylceramidase (GALC) activity were elevated above background in the internal capsule, the only subcortical structure examined.[89]

Although some studies report superior overall transduction of the brain with CSF versus systemic delivery, the intravenous route may produce an equivalent or better clinical effect. For example, dogs with mucopolysaccharidosis (MPS) VII were treated with similar doses of AAV9 intravenously or via the cisterna magna. Although CSF delivery produced higher activity of the missing lysosomal enzyme in the brain, gait function after systemic treatment was equivalent to, or better than that of CSF delivery.[90] In the current study, treated GM1 animals did not have a normal lifespan but survived 5.2 times longer than untreated cats, with a vastly improved quality of life. In fact, GM1 cats in the long-term cohort had near-normal neuromuscular function as assessed by our clinical rating scale. Their demise ultimately was caused by weight loss. Weight loss may have been due to an intermittent or chronic pancreatitis, which was confirmed histopathologically in one of the cats in the long-term cohort (8–1714) and is not necessarily related to gangliosidosis or AAV treatment because it occurs in normal members of the feline research colony. Also, pancreatitis did not occur in any of the animals treated for 16 weeks or in the additional member of the long-term cohort.

The current study uses an AAV construct that contains WPRE, which has raised concerns about toxicity.[58,91] WPRE is used to enhance transgene expression through increased cytoplasmic accumulation of the virus.[92,93] The two FDA approved AAV therapies do not include WPRE in the vector backbone,[51,94] nor do vectors in many ongoing clinical trials evaluating intravenous treatment of late-onset Pompe disease,[95] spinal muscular atrophy,[96] MPS IIIA[97] and others. When comparing βgal activity in cell culture using AAV9 vectors with and without WPRE, there was no significant difference. If anything, the vector without WPRE showed a tendency for higher βgal expression compared to the vector including WPRE. While this experiment is important in that no major differences in βgal expression were detected, performance *in vitro* may differ from results *in vivo*. To minimize animal usage in the sentient feline model, we did not evaluate the vector without WPRE in GM1 cats.

In summary, intravenous delivery of AAV9 expressing feline βgal dramatically improved quality and length of life in GM1 cats. Near-normal neurological status was maintained throughout the life of the two animals studied long-term. βGal distribution was widespread throughout the CNS and peripheral organs, reaching normal levels in the cerebellum, spinal cord, heart, liver, spleen and skeletal muscle. We also observed reduced accumulation of GM1 in the CNS. Although one treated animal developed pancreatitis ~3 years post-treatment, no other consistent indications of possible treatment toxicity or aggravated immune response were apparent clinically or histologically. The simple intravenous

injection is substantially less invasive than intracranial or CSF delivery and ultimately will be possible as an outpatient procedure. Taken together, the results support the use of AAV9 via intravenous delivery for the treatment of GM1 gangliosidosis, and these data supported an Investigational New Drug application with the US Food and Drug Administration for a first-in-human gene therapy clinical trial for GM1, which is ongoing (https://clinicaltrials.gov/ Identifier NCT03952637).

Funding

Competing interests

A.L.G., H.L.G., M.S.E. and D.R.M. are beneficiaries of a licensing agreement with Sio (formerly Axovant) Gene Therapies (New York City) based partly on this technology. M.S.E. and D.R.M. are shareholders in Lysogene (Neuilly-sur-Seine, France).

Supplementary material

Supplementary material is available at *Brain* online.

References

1. Regier DS, Tifft CJ, Rothermel CE. GLB1-related disorders. In: Adam MP, Ardinger HH, Pagon RA, eds. *GeneReviews®*. University of Washington, Seattle; 2021.

2. Meikle PJ, Fietz MJ, Hopwood JJ. Diagnosis of lysosomal storage disorders: Current techniques and future directions. *Expert Rev Mol Diagn*. 2004;4(5):677–691.

3. Okada S, O'Brien JS. Generalized gangliosidosis: Beta-galactosidase deficiency. *Science*. 1968;160(3831):1002–1004.

4. Brunetti-Pierri N, Scaglia F. GM1 gangliosidosis: Review of clinical, molecular, and therapeutic aspects. *Mol Genet Metab*. 2008; 94(4):391–396.

5. Ferreira CR, Gahl WA. Lysosomal storage diseases. *Transl Sci Rare Dis*. 2017;2(1-2):1–71.

6. Hahn CN, del Pilar Martin M, Schröder M, et al. Generalized CNS disease and massive GM1-ganglioside accumulation in mice defective in lysosomal acid beta-galactosidase. *Hum Mol Genet*. 1997;6(2):205–211.

7. Matsuda J, Suzuki O, Oshima A, et al. Beta-galactosidase-deficient mouse as an animal model for GM1-gangliosidosis. *Glycoconj J*. 1997;14(6):729–736.

8. Matsuda J, Suzuki O, Oshima A, Ogura A, Naiki M, Suzuki Y. Neurological manifestations of knockout mice with beta-galactosidase deficiency. *Brain Dev*. 1997;19(1):19–20.

9. Baker HJ Jr, Lindsey JR, McKhann GM, Farrell DF. Neuronal GM1 gangliosidosis in a Siamese cat with beta-galactosidase deficiency. *Science*. 1971;174(4011):838–839.

10. Farrell DF, Baker HJ, Herndon RM, Lindsey JR, McKhann GM. Feline GM 1 gangliosidosis: Biochemical and ultrastructural comparisons with the disease in man. *J Neuropathol Exp Neurol*. 1973;32(1):1–18.

11. Baker HJ, Lindsey JR. Animal model: Feline GM1 gangliosidosis. *Am J Pathol*. 1974;74(3):649–652.

12. Casal M, Haskins M. Large animal models and gene therapy. *Eur J Hum Genet*. 2006;14(3):266–272.

13. Vite CH, Passini MA, Haskins ME, Wolfe JH. Adeno-associated virus vector-mediated transduction in the cat brain. *Gene Ther*. 2003;10(22):1874–1881.

14. Baek RC, Broekman ML, Leroy SG, et al. AAV-mediated gene delivery in adult GM1-gangliosidosis mice corrects lysosomal storage in CNS and improves survival. *PLoS ONE*. 2010;5(10): e13468.

15. Broekman ML, Baek RC, Comer LA, Fernandez JL, Seyfried TN, Sena-Esteves M. Complete correction of enzymatic deficiency and neurochemistry in the GM1-gangliosidosis mouse brain by neonatal adeno-associated virus-mediated gene delivery. *Mol Ther*. 2007;15(1):30–37.

16. McCurdy VJ, Johnson AK, Gray-Edwards HL, et al. Sustained normalization of neurological disease after intracranial gene therapy in a feline model. *Sci Transl Med*. 2014;6(231):231ra48.

17. Dodge JC, Clarke J, Song A, et al. Gene transfer of human acid sphingomyelinase corrects neuropathology and motor deficits in a mouse model of Niemann-Pick type A disease. *Proc Natl Acad Sci USA*. 2005;102(49):17822–17827.

18. Bosch A, Perret E, Desmaris N, Heard JM. Long-term and significant correction of brain lesions in adult mucopolysaccharidosis type VII mice using recombinant AAV vectors. *Mol Ther*. 2000; 1(1):63–70.

19. Skorupa AF, Fisher KJ, Wilson JM, Parente MK, Wolfe JH. Sustained production of beta-glucuronidase from localized sites after AAV vector gene transfer results in widespread distribution of enzyme and reversal of lysosomal storage lesions in a large volume of brain in mucopolysaccharidosis VII mice. *Exp Neurol*. 1999;160(1):17–27.

20. Kaplitt MG, Feigin A, Tang C, et al. Safety and tolerability of gene therapy with an adeno-associated virus (AAV) borne GAD gene for Parkinson's disease: An open label, phase I trial. *Lancet*. 2007;369(9579):2097–2105.

21. Yang B, Li S, Wang H, et al. Global CNS transduction of adult mice by intravenously delivered rAAVrh.8 and rAAVrh.10 and nonhuman primates by rAAVrh.10. *Mol Ther*. 2014;22(7): 1299–1309.

22. Zhang H, Yang B, Mu X, et al. Several rAAV vectors efficiently cross the blood-brain barrier and transduce neurons and astrocytes in the neonatal mouse central nervous system. *Mol Ther*. 2011;19(8):1440–1448.

23. Foust KD, Nurre E, Montgomery CL, Hernandez A, Chan CM, Kaspar BK. Intravascular AAV9 preferentially targets neonatal neurons and adult astrocytes. *Nat Biotechnol*. 2009;27(1):59–65.

24. Weismann CM, Ferreira J, Keeler AM, et al. Systemic AAV9 gene transfer in adult GM1 gangliosidosis mice reduces lysosomal storage in CNS and extends lifespan. *Hum Mol Genet*. 2015; 24(15):4353–4364.

25. Duque S, Joussemet B, Riviere C, et al. Intravenous administration of self-complementary AAV9 enables transgene delivery to adult motor neurons. *Mol Ther*. 2009;17(7):1187–1196.

26. Matalon R, Surendran S, Rady PL, et al. Adeno-associated virus-mediated aspartoacylase gene transfer to the brain of knockout mouse for Canavan disease. *Mol Ther*. 2003;7(5 Pt 1):580–587.

27. Broekman ML, Comer LA, Hyman BT, Sena-Esteves M. Adeno-associated virus vectors serotyped with AAV8 capsid are more efficient than AAV-1 or -2 serotypes for widespread gene delivery to the neonatal mouse brain. *Neuroscience*. 2006;138(2): 501–510.

28. Choudhury SR, Harris AF, Cabral DJ, et al. Widespread central nervous system gene transfer and silencing after systemic delivery of novel AAV-AS vector. *Mol Ther*. 2016;24(4):726–735.

29. Schneider CA, Rasband WS, Eliceiri KW. NIH Image to ImageJ: 25 years of image analysis. *Nat Methods*. 2012;9(7):671–675.

30. Martin DR, Cox NR, Morrison NE, et al. Mutation of the GM2 activator protein in a feline model of GM2 gangliosidosis. *Acta Neuropathol*. 2005;110(5):443–450.

31. Baek RC, Martin DR, Cox NR, Seyfried TN. Comparative analysis of brain lipids in mice, cats, and humans with Sandhoff disease. *Lipids*. 2009;44(3):197–205.

32. Baek RC, Kasperzyk JL, Platt FM, Seyfried TN. N-butyldeoxygalactonojirimycin reduces brain ganglioside and GM2 content in neonatal Sandhoff disease mice. *Neurochem Int*. 2008;52(6): 1125–1133.

33. Seyfried TN, Yu RK, Miyazawa N. Differential cellular enrichment of gangliosides in the mouse cerebellum: Analysis using neurological mutants. *J Neurochem*. 1982;38(2):551–559.

34. Kasperzyk JL, El-Abbadi MM, Hauser EC, D'Azzo A, Platt FM, Seyfried TN. N-butyldeoxygalactonojirimycin reduces neonatal brain ganglioside content in a mouse model of GM1 gangliosidosis. *J Neurochem*. 2004;89(3):645–653.

35. Macala LJ, Yu RK, Ando S. Analysis of brain lipids by high performance thin-layer chromatography and densitometry. *J Lipid Res*. 1983;24(9):1243–1250.

36. Seyfried TN, Glaser GH, Yu RK. Cerebral, cerebellar, and brain stem gangliosides in mice susceptible to audiogenic seizures. *J Neurochem*. 1978;31(1):21–27.

37. Folch J, Lees M, Sloane Stanley GH. A simple method for the isolation and purification of total lipides from animal tissues. *J Biol Chem*. 1957;226(1):497–509.

38. Kasperzyk JL, d'Azzo A, Platt FM, Alroy J, Seyfried TN. Substrate reduction reduces gangliosides in postnatal cerebrum-brain-stem and cerebellum in GM1 gangliosidosis mice. *J Lipid Res*. 2005;46(4):744–751.

39. Gray-Edwards HL, Regier DS, Shirley JL, et al. Novel biomarkers of human GM1 gangliosidosis reflect the clinical efficacy of gene therapy in a feline model. *Mol Ther*. 2017;25(4):892–903.

40. Helfer-Hungerbuehler AK, Widmer S, Hofmann-Lehmann R. GAPDH pseudogenes and the quantification of feline genomic DNA equivalents. *Mol Biol Int*. 2013;2013:587680.

41. Bradbury AM, Cochran JN, McCurdy VJ, et al. Therapeutic response in feline Sandhoff disease despite immunity to intracranial gene therapy. *Mol Ther*. 2013;21(7):1306–1315.

42. Martin DR, Rigat BA, Foureman P, et al. Molecular consequences of the pathogenic mutation in feline GM1 gangliosidosis. *Mol Genet Metab*. 2008;94(2):212–221.

43. Blüml S, Seymour KJ, Ross BD. Developmental changes in choline- and ethanolamine-containing compounds measured with proton-decoupled (31)P MRS in *in vivo* human brain. *Magn Reson Med*. 1999;42(4):643–654.

44. Zhu H, Barker PB. MR spectroscopy and spectroscopic imaging of the brain. *Methods Mol Biol*. 2011;711:203–226.

45. Ross B, Bluml S. Magnetic resonance spectroscopy of the human brain. *Anat Rec*. 2001;265(2):54–84.

46. Ford TC, Crewther DP. A comprehensive review of the 1H-MRS metabolite spectrum in autism spectrum disorder. *Front Mol Neurosci*. 2016;9:14.

47. Rae CD. A guide to the metabolic pathways and function of metabolites observed in human brain 1H magnetic resonance spectra. *Neurochem Res*. 2014;39(1):1–36.

48. Bak LK, Schousboe A, Waagepetersen HS. The glutamate/GABA-glutamine cycle: Aspects of transport, neurotransmitter homeostasis and ammonia transfer. *J Neurochem*. 2006;98(3): 641–653.

49. Hinderer C, Katz N, Buza EL, et al. Severe toxicity in nonhuman primates and piglets following high-dose intravenous administration of an adeno-associated virus vector expressing human SMN. *Hum Gene Ther*. 2018;29(3):285–298.

50. Maguire AM, Russell S, Wellman JA, et al. Efficacy, safety, and durability of voretigene neparvovec-rzyl in RPE65 mutation-associated inherited retinal dystrophy: Results of phase 1 and 3 trials. *Ophthalmology*. 2019;126(9):1273–1285.

51. Mendell JR, Al-Zaidy S, Shell R, et al. Single-dose gene-replacement therapy for spinal muscular atrophy. *N Engl J Med.* 2017; 377(18):1713–1722.

52. Mondo E, Moser R, Gao G, et al. Selective neuronal uptake and distribution of AAVrh8, AAV9, and AAVrh10 in sheep after intrastriatal administration. *J Huntingtons Dis.* 2018;7(4):309–319.

53. Pardridge WM. Drug and gene delivery to the brain: The vascular route. *Neuron.* 2002;36(4):555–558.

54. Regier DS, Kwon HJ, Johnston J, et al. MRI/MRS as a surrogate marker for clinical progression in GM1 gangliosidosis. *Am J Med Genet A.* 2016;170(3):634–644.

55. Erol I, Alehan F, Pourbagher MA, Canan O, Vefa Yildirim S. Neuroimaging findings in infantile GM1 gangliosidosis. *Eur J Paediatr Neurol.* 2006;10(5-6):245–248.

56. Rockwell HE, McCurdy VJ, Eaton SC, et al. AAV-mediated gene delivery in a feline model of Sandhoff disease corrects lysosomal storage in the central nervous system. *ASN Neuro.* 2015; 7(2):175909141556990.

57. McCurdy VJ, Rockwell HE, Arthur JR, et al. Widespread correction of central nervous system disease after intracranial gene therapy in a feline model of Sandhoff disease. *Gene Ther.* 2015; 22(2):181–189.

58. Golebiowski D, van der Bom IMJ, Kwon CS, et al. Direct intracranial injection of AAVrh8 encoding monkey beta-*N*-acetylhexosaminidase causes neurotoxicity in the primate brain. *Hum Gene Ther.* 2017;28(6):510–522.

59. Somanathan S, Calcedo R, Wilson JM. Adenovirus-antibody complexes contributed to lethal systemic inflammation in a gene therapy trial. *Mol Ther.* 2020;28(3):784–793.

60. Baker AH, Herzog RW. Did dendritic cell activation, induced by adenovirus-antibody complexes, play a role in the death of Jesse Geisinger? *Mol Ther.* 2020;28(3):704–706.

61. Philippidis A. After third death, Audentes' AT132 remains on clinical hold. *Hum Gene Ther.* 2020;31(17-18):908–910.

62. Elmore ZC, Oh DK, Simon KE, Fanous MM, Asokan A. Rescuing AAV gene transfer from neutralizing antibodies with an IgG-degrading enzyme. *JCI Insight.* 2020;5(19):e139881.

63. Leborgne C, Barbon E, Alexander JM, et al. IgG-cleaving endopeptidase enables in vivo gene therapy in the presence of anti-AAV neutralizing antibodies. *Nat Med.* 2020;26(7):1096–1101.

64. Orlowski A, Katz MG, Gubara SM, Fargnoli AS, Fish KM, Weber T. Successful transduction with AAV vectors after selective depletion of anti-AAV antibodies by immunoadsorption. *Mol Ther Methods Clin Dev.* 2020;16:192–203.

65. Corti M, Cleaver B, Clément N, et al. Evaluation of readministration of a recombinant adeno-associated virus vector expressing acid alpha-glucosidase in Pompe disease: Preclinical to clinical planning. *Hum Gene Ther Clin Dev.* 2015;26(3):185–193.

66. Samoylova TI, Martin DR, Morrison NE, et al. Generation and characterization of recombinant feline beta-galactosidase for preclinical enzyme replacement therapy studies in GM1 gangliosidosis. *Metab Brain Dis.* 2008;23(2):161–173.

67. Blyth BJ, Farhavar A, Gee C, et al. Validation of serum markers for blood-brain barrier disruption in traumatic brain injury. *J Neurotrauma.* 2009;26(9):1497–1507.

68. Broekman ML, Tierney LA, Benn C, Chawla P, Cha JH, Sena-Esteves M. Mechanisms of distribution of mouse beta-galactosidase in the adult GM1-gangliosidosis brain. *Gene Ther.* 2009; 16(2):303–308.

69. Bevan AK, Duque S, Foust KD, et al. Systemic gene delivery in large species for targeting spinal cord, brain, and peripheral tissues for pediatric disorders. *Mol Ther.* 2011;19(11):1971–1980.

70. Samaranch L, Salegio EA, San Sebastian W, et al. Adeno-associated virus serotype 9 transduction in the central nervous system of nonhuman primates. *Hum Gene Ther.* 2012;23(4):382–389.

71. Gray SJ, Nagabhushan Kalburgi S, McCown TJ, Jude Samulski R. Global CNS gene delivery and evasion of anti-AAV-neutralizing antibodies by intrathecal AAV administration in non-human primates. *Gene Ther.* 2013;20(4):450–459.

72. Hordeaux J, Hinderer C, Buza EL, et al. Safe and sustained expression of human iduronidase after intrathecal administration of adeno-associated virus serotype 9 in infant rhesus monkeys. *Hum Gene Ther.* 2019;30(8):957–966.

73. Borel F, Adams E, Mueller C. Intrathecal delivery of AAV vectors in cynomolgus macaques for CNS gene therapy and gene expression analysis in microdissected motor neurons. *Methods Mol Biol.* 2019;1937:295–303.

74. Bey K, Deniaud J, Dubreil L, et al. Intra-CSF AAV9 and AAVrh10 administration in nonhuman primates: Promising routes and vectors for which neurological diseases? *Mol Ther Methods Clin Dev.* 2020;17:771–84.

75. Hinderer C, Nosratbakhsh B, Katz N, Wilson JM. A single injection of an optimized adeno-associated viral vector into cerebrospinal fluid corrects neurological disease in a murine model of GM1 gangliosidosis. *Hum Gene Ther.* 2020;31(21-22):1169–1177.

76. Bucher T, Dubreil L, Colle MA, et al. Intracisternal delivery of AAV9 results in oligodendrocyte and motor neuron transduction in the whole central nervous system of cats. *Gene Ther.* 2014;21(5):522–528.

77. Bucher T, Colle MA, Wakeling E, et al. scAAV9 intracisternal delivery results in efficient gene transfer to the central nervous system of a feline model of motor neuron disease. *Hum Gene Ther.* 2013;24(7):670–682.

78. Naidoo J, Stanek LM, Ohno K, et al. Extensive transduction and enhanced spread of a modified AAV2 capsid in the non-human primate CNS. *Mol Ther.* 2018;26(10):2418–2430.

79. Donsante A, McEachin Z, Riley J, et al. Intracerebroventricular delivery of self-complementary adeno-associated virus serotype 9 to the adult rat brain. *Gene Ther.* 2016;23(5):401–407.

80. Bey K, Deniaud J, Dubreil L, et al. Intra-CSF AAV9 and AAVrh10 administration in nonhuman primates: Promising routes and vectors for which neurological diseases? *Mol Ther Methods Clin Dev.* 2020;17:771–784.

81. Haurigot V, Marco S, Ribera A, et al. Whole body correction of mucopolysaccharidosis IIIA by intracerebrospinal fluid gene therapy. *J Clin Invest.* 2013;123(8):3254–3271.

82. Yoon SY, Bagel JH, O'Donnell PA, Vite CH, Wolfe JH. Clinical improvement of alpha-mannosidosis cat following a single cisterna magna infusion of AAV1. *Mol Ther.* 2016;24(1):26–33.

83. Hinderer C, Bell P, Gurda BL, et al. Intrathecal gene therapy corrects CNS pathology in a feline model of mucopolysaccharidosis I. *Mol Ther.* 2014;22(12):2018–2027.

84. Deverman BE, Pravdo PL, Simpson BP, et al. Cre-dependent selection yields AAV variants for widespread gene transfer to the adult brain. *Nat Biotechnol.* 2016;34(2):204–209.

85. Yoon SY, Hunter JE, Chawla S, et al. Global CNS correction in a large brain model of human alpha-mannosidosis by intravascular gene therapy. *Brain.* 2020;143(7):2058–2072.

86. Liguore WA, Domire JS, Button D, et al. AAV-PHP.B administration results in a differential pattern of CNS biodistribution in non-human primates compared with mice. *Mol Ther.* 2019; 27(11):2018–2037.

87. Hordeaux J, Wang Q, Katz N, Buza EL, Bell P, Wilson JM. The neurotropic properties of AAV-PHP.B are limited to C57BL/6J mice. *Mol Ther.* 2018;26(3):664–668.

88. Matsuzaki Y, Konno A, Mochizuki R, et al. Intravenous administration of the adeno-associated virus-PHP.B capsid fails to upregulate transduction efficiency in the marmoset brain. *Neuroscience Lett.* 2018;665:182–188.

89. Bradbury AM, Bagel JH, Nguyen D, et al. Krabbe disease successfully treated via monotherapy of intrathecal gene therapy. *J Clin Invest*. 2020;130(9):4906–4920.

90. Gurda BL, De Guilhem De Lataillade A, Bell P, et al. Evaluation of AAV-mediated gene therapy for central nervous system disease in canine mucopolysaccharidosis VII. *Mol Ther*. 2016;24(2): 206–216.

91. Patricio MI, Barnard AR, Orlans HO, McClements ME, MacLaren RE. Inclusion of the woodchuck hepatitis virus posttranscriptional regulatory element enhances AAV2-driven transduction of mouse and human retina. *Mol Ther Nucleic Acids*. 2017;6:198–208.

92. Paterna JC, Moccetti T, Mura A, Feldon J, Bueler H. Influence of promoter and WHV post-transcriptional regulatory element on AAV-mediated transgene expression in the rat brain. *Gene Ther*. 2000;7(15):1304–1311.

93. Loeb JE, Cordier WS, Harris ME, Weitzman MD, Hope TJ. Enhanced expression of transgenes from adeno-associated virus vectors with the woodchuck hepatitis virus posttranscriptional regulatory element: Implications for gene therapy. *Hum Gene Ther*. 1999;10(14):2295–2305.

94. Bennicelli J, Wright JF, Komaromy A, et al. Reversal of blindness in animal models of Leber congenital amaurosis using optimized AAV2-mediated gene transfer. *Mol Ther*. 2008;16(3): 458–465.

95. Sun B, Zhang H, Franco LM, et al. Efficacy of an adeno-associated virus 8-pseudotyped vector in glycogen storage disease type II. *Mol Ther*. 2005;11(1):57–65.

96. Al-Zaidy SA, Kolb SJ, Lowes L, et al. AVXS-101 (Onasemnogene Abeparvovec) for SMA1: Comparative study with a prospective natural history cohort. *J Neuromuscul Dis*. 2019;6(3):307–317.

97. Hocquemiller M, Hemsley KM, Douglass ML, et al. AAVrh10 vector corrects disease pathology in MPS IIIA mice and achieves widespread distribution of SGSH in large animal brains. *Mol Ther Methods Clin Dev*. 2020;17:174–187.